Atmospheric Environment 190 (2018) 135–145

Contents lists available at ScienceDirect

Atmospheric Environment

journal homepage: www.elsevier.com/locate/atmosenv

Assessment of a high-resolution NO_X emission inventory using satellite observations: A case study of southern Jiangsu, China

Yu Zhao[a,b,*], Yinmin Xia[a], Yaduan Zhou[a]

[a] State Key Laboratory of Pollution Control & Resource Reuse and School of the Environment, Nanjing University, 163 Xianlin Ave., Nanjing, Jiangsu 210023, China
[b] Jiangsu Collaborative Innovation Center of Atmospheric Environment and Equipment Technology (CICAEET), Nanjing University of Information Science & Technology, Jiangsu 210044, China

ARTICLE INFO

Keywords:
Nitrogen oxide
Satellite observation
Emissions
Chemistry transport modeling

ABSTRACT

To evaluate the bottom-up NO_X emission inventories with different data sources and spatial scales, an updated product of tropospheric NO_2 vertical column densities (VCDs) from Ozone Monitoring Instrument (OMI), POMINO, was applied in chemistry transport modeling (CTM) and Gaussian function model for southern Jiangsu, a typical developed and polluted region in eastern China. Compared to the national emission inventory (MEIC), better correlation was found between spatial distributions of the high-resolution provincial inventory (JS) and POMINO VCDs. When applied in CTM, the simulated VCDs using JS were closer to POMINO data than those using MEIC, indicating the advantage of the provincial inventory that incorporated detailed information of individual plants. The simulated VCDs, however, were generally larger than observed ones, particularly for regions with high NO_2 levels, partly because the improved NO_X control measures for power sector were not fully considered in both national and provincial inventories. The "top-down" NO_X emissions were estimated for four cities/city combinations in southern Jiangsu, using a Gaussian function model based on POMINO NO_2 VCDs. The results were found to be most consistent with the estimates in JS among bottom-up inventories with different data sources. To further harmonize emissions and satellite observations at relatively small spatial scale, the on-line emission measurement data for individual plants are recommended for emission inventory development, and the products of satellite observation data with finer horizontal resolution are encouraged.

1. Introduction

As precursors of ambient ozone and nitrate aerosols, nitrogen oxides (NO_X) are considered as crucial air pollutants in tropospheric chemistry (Seinfeld and Pandis, 2006). Coming largely from thermal power and transportation, NO_X indicates the scales of economy and fossil fuel combustion for areas with intensive anthropogenic activities like eastern China. With serious air pollution, China has been conducting series of measures to reduce pollutant emissions, and dramatic changes in amount and spatiotemporal pattern of emissions are expected across the country (Zhao et al., 2014; Xia et al., 2016; Liu et al., 2016a; van der A et al., 2017). Such changes, however, could hardly be tracked through the bottom-up emission inventories in which information of individual emission sources were unavailable on a timely and instant basis through routine statistics (Zhao et al., 2015).

To better understand the emissions of developed regions in China, city- and provincial-scale inventories were developed integrating the best knowledge of local emission sources. Advantages of those inventories on air quality simulation were then evaluated through chemistry transport modeling (CTM), indicated by the discrepancies between simulated and observed surface concentrations of selected pollutants (Zheng et al., 2009; Wang et al., 2010; Zhao et al., 2015; Zhou et al., 2017; Liu et al., 2018). Currently, some limitations existed when ground observations were used in evaluation of city- and provincial-scale inventories across China. As ground stations of the national monitoring network in China are commonly located in urban areas, observation data reflecting regional levels of air pollutants were hardly available to public. Therefore, the spatial patterns of emissions could not easily been tested for primary pollutants like NO_X, limited by the numbers and representativeness of observation stations in a given area. Moreover, as the observation data at limited stations in urban areas could not indicate the condition for the whole city, they could hardly be applied to derive "top-down" estimates of primary pollutant emissions at city level, limiting the assessment of bottom-up

* Corresponding author. State Key Laboratory of Pollution Control & Resource Reuse and School of the Environment, Nanjing University, 163 Xianlin Ave., Nanjing, Jiangsu 210023, China.
E-mail address: yuzhao@nju.edu.cn (Y. Zhao).

https://doi.org/10.1016/j.atmosenv.2018.07.029
Received 30 October 2017; Received in revised form 11 July 2018; Accepted 13 July 2018
Available online 20 July 2018

inventories. Besides ground measurements, therefore, observation data from other sources are needed to help better understanding the emissions of typical air pollutants.

Satellites have been used for tropospheric NO_2 detection with satisfying spatial coverage (Richter et al., 2005; Boersma et al., 2007; Krotkov et al., 2016). At continental and national scales, NO_2 vertical column densities (VCDs) from Ozone Monitoring Instrument (OMI) were applied to constrain the emissions and to detect the effectiveness of air quality policy in China (Mijling et al., 2013; van der A et al., 2017). OMI-derived VCDs were also compared against simulated VCDs with CTM based on various emission inventories, and the accuracies of those inventories were then evaluated for different regions across the country (Han et al., 2015). Besides large spatial scale, satellite-derived VCDs were used in evaluating the emissions or pollution levels for point sources (e.g., power plant) and cities (Duncan et al., 2013; de Foy et al., 2016). In particular, the Gaussian function model was developed in a top-down methodology to estimate the emissions of isolated point sources (Lu et al., 2013; de Foy et al., 2015) or cities (Beirle et al., 2011; Lu et al., 2015; Zhang et al., 2018) based on OMI observations, although uncertainties existed in the methodology (de Foy et al., 2014). Furthermore, Liu et al. (2016b) modified the approach accounting for the effect of interfering sources within small distances, and then estimated the lifetime and emissions of NO_X of given power plants and cities located in heterogeneously polluted background in China. Such method was applied to quantify the inter-annual trends in NO_X emissions for selected Chinese cities (Liu et al., 2017). Although the CTM and Gaussian function have been applied in different countries, comprehensive analysis of NO_X emissions based on satellite observations is still lacking at regional scale, and the advantage of local inventories on air quality research is insufficiently evaluated.

In this work, therefore, we select southern Jiangsu, a region with developed economy and industry in eastern China (see Fig. 1), and combine satellite observations, chemistry transport model and Gaussian dispersion function model to evaluate the bottom-up emission inventories. Jiangsu was the first ranked province in gross domestic product (GDP) per capita in China (NBS, 2016a), and accounted for 7.5%, 7.7%, 10.2%, and 13.7% of the country's power generation, cement, pig iron, and crude steel production in 2015, respectively (NBS, 2016b). Intensive industry resulted in heavy air pollution in recent years, particularly in south of the province, and tightened measures have been applied to reduce emissions. Based on satellite-derived VCDs, we first compare spatial patterns of NO_X emissions in two inventories at different scales. CTM was further applied to test the advantage of the provincial inventory prior to the downscaled national one. With modified Gaussian function, finally, the lifetimes and emission rates of NO_X for individual cities were calculated, and such top-down results were used for evaluation of bottom-up emissions from different data sources. The current study provides a perspective from satellite observations to examine the NO_X emissions at regional and city scales, and provides a comprehensive understanding in typical air pollutant emissions together with our previous studies that evaluated local inventories based on ground observations and CTM (Zhao et al., 2015, 2017a; Zhou et al., 2017).

2. Data and methods

2.1. Emission and satellite data

Two bottom-up emission inventories for 2012 were included in the analysis. One is the Multi-resolution Emission Inventory for China (MEIC, http://www.meicmodel.org/), developed by Tsinghua University. This national inventory provides annual emissions by sector (power, industry, transportation, residential, and agricultural) for 31 Chinese provinces (two special administrative regions Hong Kong and Macau not included). The horizontal resolution of MEIC is flexible and can be determined by the users, with the finest at 0.25° longitude × 0.25° latitude available to public. In MEIC, the emissions from power sector were calculated with a unit-based method, integrating the best available information of individual plants (Liu et al., 2015). For other sectors, the emissions were estimated at provincial or county level and then allocated into grids using different proxies (population and road net, etc). The other inventory is a provincial inventory for Jiangsu, developed in our previous work (Zhou et al., 2017; http://www.airqualitynju.com/En/Data/List/Data%20download). In the inventory, most plants of power and industry sectors were identified as point sources, and the information on geophysical location, emission factors and activity data for each plant was investigated and modified through official environmental statistics, Pollution Source Census (internal data), and on-site surveys on large emitters. Improved estimation and spatial distribution of emissions could thus be expected. The horizontal resolution of the inventory reaches 3 × 3 km. Hereinafter we mention this high-resolution inventory for Jiangsu as JS inventory. In our previous work, emission inventories with varied spatial scales for Jiangsu (MEIC, JS, and another regional inventory by Fu et al. (2013)) were evaluated through CTM, and the best model performance was achieved for JS inventory, indicated by available ground observations of NO_2 and O_3 (Zhao et al., 2017a; Zhou et al., 2017).

For satellite data in China, Lin et al. (2014) modified the calculation

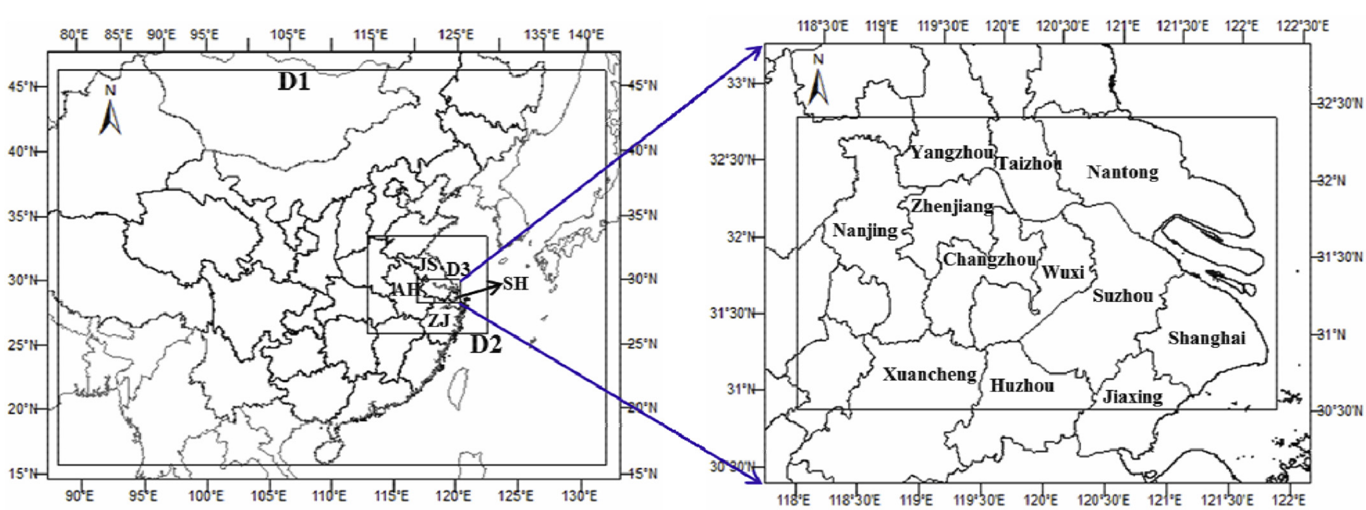

Fig. 1. Location of Jiangsu Province and the three nested domains for CMAQ modeling. JS, ZJ, AH and SH indicate the province of Jiangsu, Zhejiang, Anhui, and the city of Shanghai, respectively.

of air mass factor (AMF) considering the effect of aerosols on solar radiation and that of local topography on surface albedo. An updated product of NO_2 VCDs, POMINO, was then developed based on OMI observations. Lin et al. (2014) compared POMINO data with the ground-based observations through multi axis differential optical absorption spectroscopy (MAX-DOAS) at three observation sites in eastern China, and found a strong correlation between MAX-DOAS observations and POMINO ($R^2 = 0.96$). Therefore, we applied the daily level-3 product of POMINO with a horizontal resolution at 0.25° × 0.25° for emission estimation and evaluation. As clouds reduce the accuracy of satellite measurements, only data with cloud fraction ≤ 0.2 were applied. Wind fields were taken from the European Center for Medium-range Weather Forecast (ECMWF) ERA-Interim reanalysis (http://www.ecmwf.int/en/research/climate-reanalysis/era-interim), and the averaged information under 500 m was used. Although the ideal threshold for calm wind was under 5 km/h (i.e., 1.4 m/s), the spatial distribution of VCDs would still be close to symmetric when the wind speed reached 10 km/h (2.8 m/s), implying a moderate influence on emission estimates (Fioletov et al., 2015; Liu et al., 2016b). Due to limited satellite data, we defined the calm wind conditions as wind speed below 2.5 m/s, to be a good compromise of sufficient sample size for calculation of NO_2 line densities (see Section 2.3 for details) for both calm and windy conditions. Shown in Fig. 2 is the NO_2 VCD from POMINO under calm conditions during Jan 2010–Aug 2014.

2.2. Air quality modeling

The Models-3/Community Multi-scale Air Quality (CMAQ) version 4.7.1 was applied to evaluate the emission inventories for Jiangsu. As shown in Fig. 1, the three one-way nested domain modeling was conducted, and the spatial resolutions were set at 27, 9 and 3 km respectively in Lambert Conformal Conic projection, centered at (110°E, 34°N) with the two true latitudes 25°N and 40°N. The mother domain (D1, 180 × 130 cells) covered most part of China, Japan and the whole Korea and part of other countries. Jiangsu, Zhejiang, Shanghai, Anhui and parts of other provinces were at the second modeling region (D2, 118 × 97 cells). The third (D3, 124 × 70 cells) covered the mega city Shanghai and six most developed cities in southern Jiangsu including Nanjing, Changzhou, Zhenjiang, Wuxi, Suzhou and Nantong. Anthropogenic emissions used for domains D1 and D2 were obtained from MEIC with an original spatial resolution of 0.25° × 0.25°. The spatial

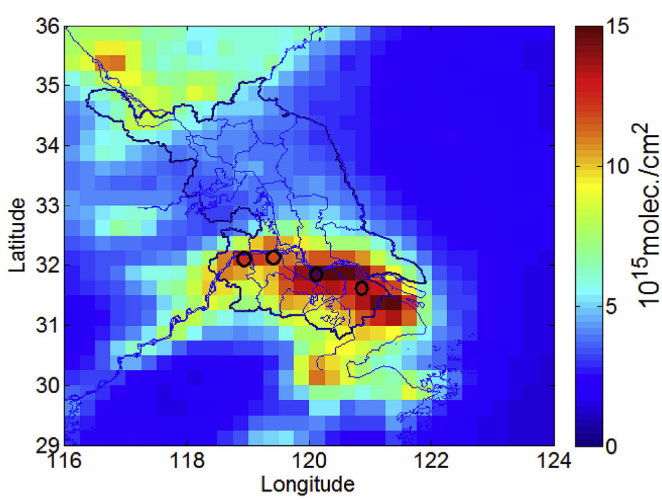

Fig. 2. NO_2 VCDs from POMINO in Jiangsu under calm wind condition (judged within the area 30–33°N, 118–122°E) from 2010 to 2014. The circles indicate the centers of concerned cities/city combinations: Nanjing (32.125°N, 118.875°E), Zhenjiang + Yangzhou (32.125°N, 119.375°E), Changzhou + Wuxi (31.875°N, 120.125°E), and Suzhou (31.625°N, 120.875°E).

distribution of Chinese population for 2012 at a horizontal resolution at 1 × 1 km was applied to relocate MEIC emissions to each modeling domain. For Jiangsu domain in D3, the downscaled MEIC according to the population density and JS inventory were used to test the modeling performance. The meteorological fields were provided by the Weather Research and Forecasting Model (WRF) version 3.4, and the outputs were transferred by meteorology chemistry interface professor (MCIP) version 4.2 into the chemistry transport module in CMAQ (CCTM). Other details of model settings were explained in our previous work including chemistry mechanisms, emissions of natural origin, and evaluation of meteorology field simulation (Zhou et al., 2017). Among typical months in different seasons, relatively sufficient NO_2 VCDs from POMINO and satisfying meteorology simulation were found for April and October 2012 in Jiangsu (Zhou et al., 2017; Zhao et al., 2017a). The two months were thus selected as CTM period, to eliminate the uncertainty from satellite observation and meteorology simulation in evaluation of emission inventories through CTM. The first five days of each month were chosen as the spin-up period to provide initial conditions for later simulations.

The NO_2 VCD from CMAQ was obtained by integrating the simulated NO_2 concentrations from ground layer to the 23rd vertical layer (0.094 atm) in the CTM, as expressed in Eqs (1) and (2):

$$n_{NO2} = \sum_{k=1}^{23} m_k \times \Delta H_k \times 100 \tag{1}$$

$$\Delta H_k = H \times \ln\left(\frac{p_k}{p_{k+1}}\right) \tag{2}$$

where n_{NO2} is the NO_2 VCD from CMAQ model (molec./cm^2); m_k is the simulated NO_2 concentrations at vertical layer k in the CMAQ (molec./cm^3); ΔH is the height of layer k (m); H represents the height when the pressure of atmosphere declines to 1/e of the original value; and p is the air pressure.

2.3. Top-down estimation of city-level NO_X emissions

As shown in Fig. 2, the NO_2 hotspots included Nanjing, Zhenjiang + Yangzhou, Changzhou + Wuxi, and Suzhou in southern Jiangsu. As the spatial distribution of NO_X emissions was not strongly associated with administrative division but locations of emission sources, we combined cities that shares common hotspots of NO_2 VCDs as one region. We followed the method by Liu et al. (2016b) and applied a modified Gaussian function model to derive the top-down estimates for city-level NO_X emissions. As the cities were located in a heterogeneously polluted background, the distribution of NO_2 VCDs under calm wind conditions was assumed as an indicator for the distribution of emissions, instead of considering the city as a single point source. Lifetime could then be obtained according to the difference between the NO_2 patterns under wind and calm conditions. In the model, one-dimensional NO_2 line densities (NO_2 per cm) can be calculated as function of distance for each wind direction sector separately by integrating the mean NO_2 VCDs (NO_2 per cm^2) perpendicular to the wind direction (Beirle et al., 2011). A model function $N(x)$ was used to fit the observed line densities of NO_2:

$$N(x) = E \times [e \otimes C](x) + B \tag{3}$$

$$e(x) = \exp\left(-\frac{x - X}{x_0}\right) \text{ for } x \geq X, \text{ 0 otherwise} \tag{4}$$

where E and B are included respectively as the scaling factor and offset accounting for possible systematic differences between windy and calm wind conditions, X is the location of the source (relative to the a priori coordinates of the site under investigation), x_0 is the e-folding distance downwind, and $C(x)$ is the NO_2 patterns observed under calm conditions. In the model, x_0 can be estimated based on the difference between NO_2 patterns under windy and calm conditions. In this work, the

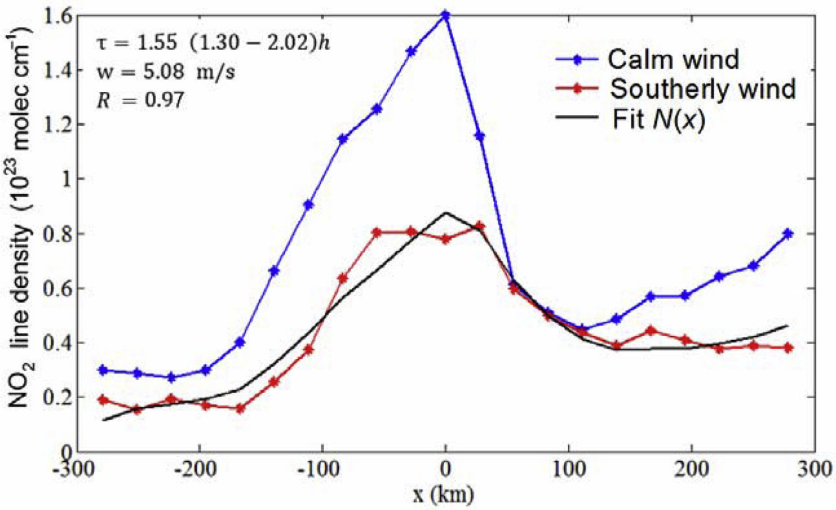

(a)

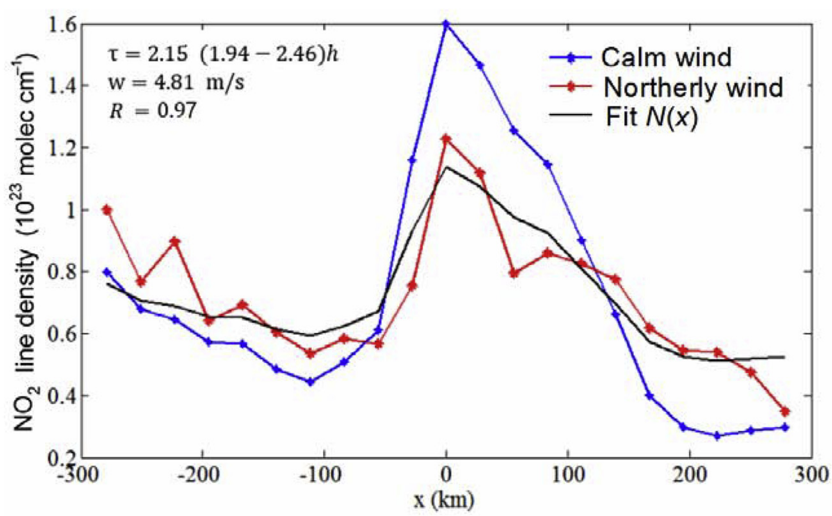

(b)

Fig. 3. NO_2 line densities around Nanjing for calm (blue) and southerly (a) and northerly (b) wind direction sectors (red) as a function of the distance x to Nanjing center. Positive and negative directions of x axis indicated directions along and opposite the wind direction, respectively. Grey lines indicate the fit result $N(x)$ (see Eq. (3)). w and τ represent the net mean wind speed (windy – calm) from ECMWF and the life time of NO_2, respectively. (For interpretation of the references to colour in this figure legend, the reader is referred to the Web version of this article.)

dominating wind directions for southern Jiangsu, i.e., southerly, northerly, southeasterly and northwesterly wind sectors were considered in determination of line densities, and only those with sufficient data from satellite observations were included. The criterion was that the missing data were less than 10% in the across-wind integration interval and less than 20% in the fit interval along wind direction. We set the fit interval in wind direction to 600 km and the across-wind integration interval to 125 km. The mean lifetime of NO_2 can be calculated by dividing x_0 by w, the mean wind speed. As an example, Fig. 3 illustrates the observed line densities for calm (blue) and wind (red) around Nanjing and the fitted model function $N(x)$ (grey) for southerly (Fig. 3a) and northerly wind conditions (Fig. 3b). Results for other wind sectors could not be obtained attributed to missing data.

The emission rate of NO_X was calculated by dividing the total mass of NO_X by lifetime. Following Liu et al. (2016b), we estimated the total mass of NO_2 based on line densities under calm wind conditions, $g(x)$:

$$g_i(x) = A \times \frac{1}{\sqrt{2\pi}\sigma_i} \exp\left(-\frac{(x-X)^2}{2\sigma_i^2}\right) + a_i + b_i x \tag{5}$$

where A is the total mass of NO_2 in the area of interest; i represents wind direction sectors northeast–southwest and south–north (opposite wind direction sectors were combined); σ_i is the standard deviation of $g_i(x)$, and $a_i + b_i x$ represents the background field. In this work, line densities were integrated from the NO_2 VCDs in across-wind direction with an interval of 40 km. As the typical concentration ratio of NO to NO_2 was 0.32 at noon in urban (Seinfeld and Pandis, 2006), the fitted A from Eq. (5) was scaled by a factor of 1.32 to obtain the mass of NO_X following Beirle et al. (2011) and Liu et al. (2016b).

3. Results and discussions

3.1. Spatial patterns of NO_X emissions and satellite-based NO_2 VCDs

The Jiangsu's NO_X emissions in 2012 were calculated at 1615 Gg in JS inventory, and power, industry, residential and transportation sector contributed 42%, 32%, 2% and 24% to the total emissions, respectively (Zhou et al., 2017). The emissions in MEIC was 22% larger than those in JS, and the analogue numbers for sector contributions were 37%, 39%, 2%, and 22%, respectively. The spatial distributions of emissions in MEIC and JS inventories were compared to that of monthly means of POMINO NO_2 VCDs in summer (May–September) 2012 over Jiangsu. To ease the comparison and correlation analysis, the gridded emissions were reallocated to the 0.25° × 0.25° grid system consistent with POMINO, i.e., emissions were aggregated into the 0.25° × 0.25° grid accounting for the areas of the 3 × 3 km grids that overlap the 0.25° × 0.25° grid receiving the aggregation. Compared to cold seasons, the lifetime of NO_2 in atmosphere is shorter in summer attributed to the enhanced photochemical reaction under high temperature, and accumulation of primary emissions is more difficult under strong air convection. In this case, the retrieved VCDs could serve as an appropriate indicator for emissions. Moreover, the summer prevailing wind in Jiangsu was from southeast where Shanghai and Zhejiang are located (see Fig. 1 for the locations). Given the relatively lower emissions in latter two regions (Xia et al., 2016), the local sources were expected to play an important role in pollution formation for Jiangsu, and evaluation of primary emissions with satellite observations could be further justified (Mijling et al., 2013).

Fig. 4a and c illustrates the spatial distribution of JS and MEIC NO_X emissions in 2012, respectively. Both JS and MEIC inventories captured the hotspots of NO_X emissions in southern Jiangsu (particularly along the Yangtze River) where economic activities and industrial plants were intensively distributed. The total correlation coefficients between VCDs and emissions were calculated at 0.69 and 0.68 for JS and MEIC inventories. As JS inventory included detailed information of industrial plants, improvement in emission estimation was ideally expected compared to MEIC. Such improvement, however, could not be suggested by the very close correlation coefficients. At relatively coarse horizontal resolution, the difference between the national (MEIC) and provincial inventories (JS) were hard to detect, and the accuracy and applicability of the national inventory could be partly confirmed through the comparison.

To further analyze the spatial distribution of emissions, correlation coefficients between VCDs and emissions were separately calculated for grids in different VCD intervals, i.e., $> 10 \times 10^{15}$ mol./cm^2 (around top 10%), 5–10 $\times 10^{15}$ mol./cm^2 (around 10–55%), and $\leq 5 \times 10^{15}$ mol./cm^2 (around last 55%), and the results were shown in Fig. 4b and d for JS and MEIC, respectively. For all the intervals, larger correlation coefficients for JS were found than those for MEIC, indicating that the spatial distribution of emissions in the high-resolution provincial inventory was more consistent with satellite-derived VCDs than that in the national inventory. Compared to JS inventory, larger slopes between emissions and VCDs were found for MEIC in high VCD intervals, but smaller in low intervals. The contrast implies that MEIC tended to

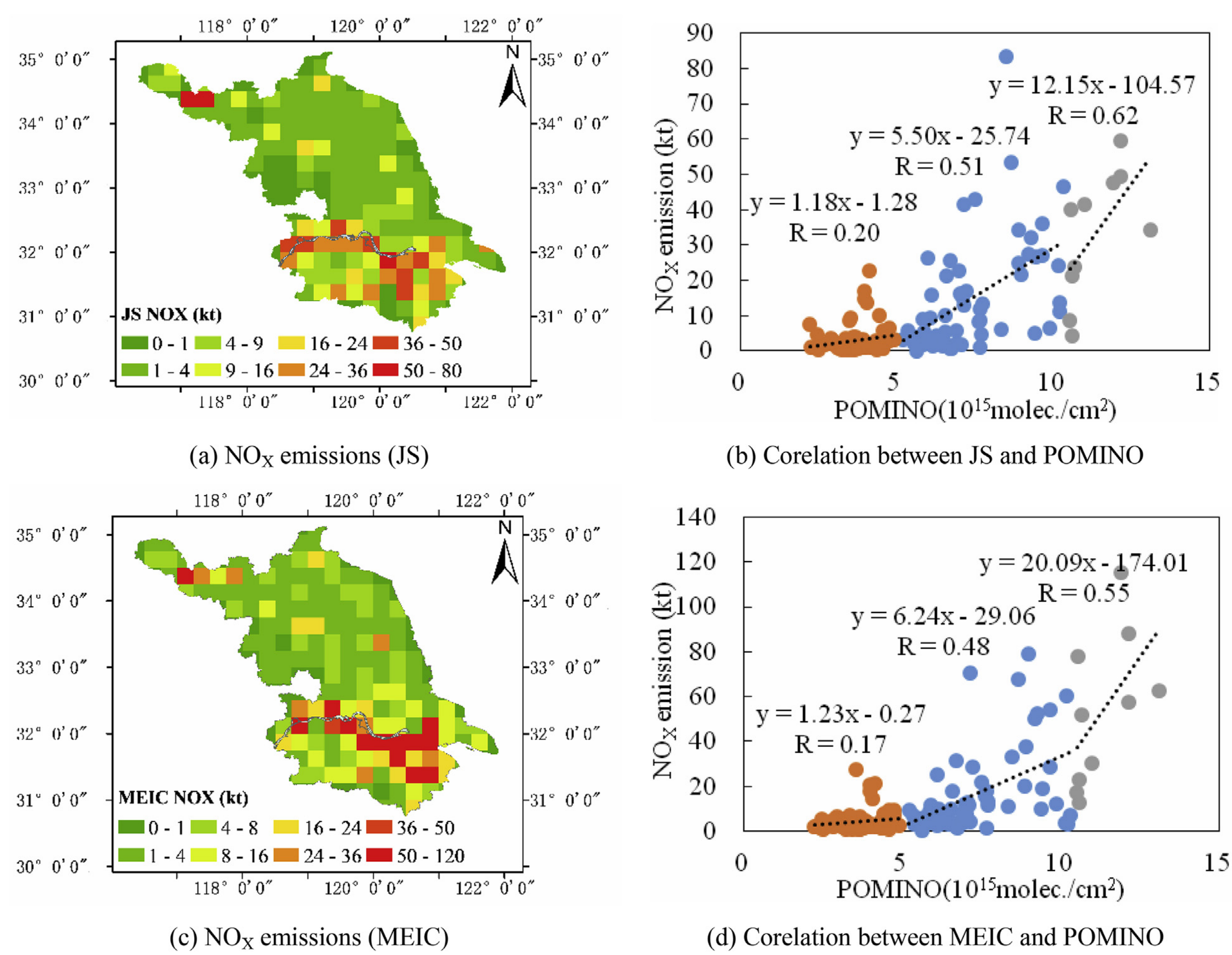

Fig. 4. Spatial distributions of NO_X emissions in JS (a) and MEIC inventories (c) at a horizontal resolution of 0.25° × 0.25° and their correlations with POMINO by NO_2 VCD interval (b and d). Dotted lines in panels b and d indicate the fitted linear regression lines.

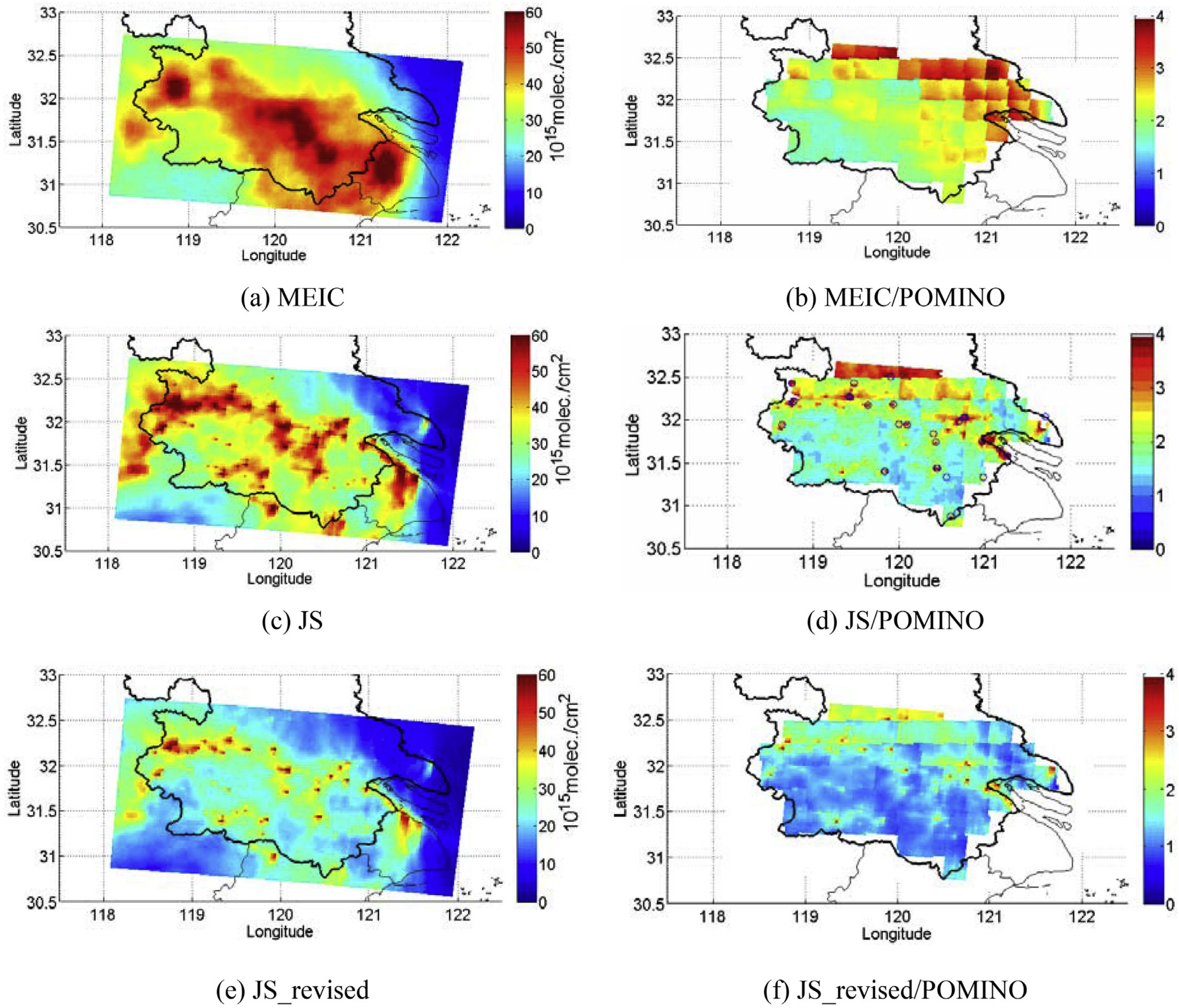

Fig. 5. Simulated NO_2 VCDs from CMAQ using MEIC (a), JS (c), and JS_revised inventories (e), and ratios of simulated to observed VCDs from POMINO (b, d, and e) for October 2012. The horizontal spatial resolution is 3 × 3 km. Hollow circles in panel d indicate the locations of power plants with SCR installed.

calculate larger emissions for high-polluted regions. It might be because the benefits on NO_X emission abatement from certain air pollutant control devices installed on big plants (e.g., selective catalytic reduction (SCR) on power sector) were not fully considered in MEIC. More discussions will follow in Section 3.2. The poorest correlation was found in the lowest VCD interval ($\leq 5 \times 10^{15}$ mol./cm^2) for both JS and MEIC inventories, indicating that improvement on emission estimation for small sources (e.g., small industrial plants and residential combustion) was still in great needed. Compared to big industrial plants that were relatively well documented, it is different to carefully track important changes on small sources all the time, e.g., closure or retrofitting. Attributed mainly to missing or incorrect information, therefore, accurate and timely emission estimation for small sources were of great challenges.

3.2. Evaluation of NO_X emissions through CTM and satellite observations

Fig. 5a and c shows the monthly mean of tropospheric NO_2 VCDs for October 2012 from CMAQ simulation based on MEIC and JS inventories, respectively. Downscaled from 0.25° × 0.25° to 3 × 3 km, the MEIC inventory in D3 could hardly identify the big power and industrial plants with relatively large emissions. As a result, the simulated hotspots of NO_2 VCDs were widely distributed in the modeling domain and commonly consistent with the locations of big cities along the Yangtze River (Fig. 5a). In contrast, notably outstanding VCDs were simulated based on JS inventory, indicating the effects of large point sources (Fig. 5c). Fig. 5b and d illustrates the spatial distributions of the ratios of simulated to POMINO NO_2 VCDs for MEIC and JS inventories, respectively. NO_2 VCDs from POMINO were evenly downscaled from 0.25° × 0.25° to 3 × 3 km, to be consistent with CMAQ simulation. Larger VCDs from CMAQ simulation than those from satellite observations were generally found in high-polluted areas, consistent with the locations of big power plants with SCR installed (indicated by the circles in Fig. 5d). Overestimation in NO_X emissions of power sector were thus implied for Jiangsu province in current available inventories. As illustrated in Fig. 6, similar results were also found for April, that NO_2 VCDs simulated with JS inventory were commonly smaller than those simulated with MEIC, and that the simulated VCDs with JS were closer to POMINO than those with MEIC.

Linear regression analysis was conducted between NO_2 VCDs from

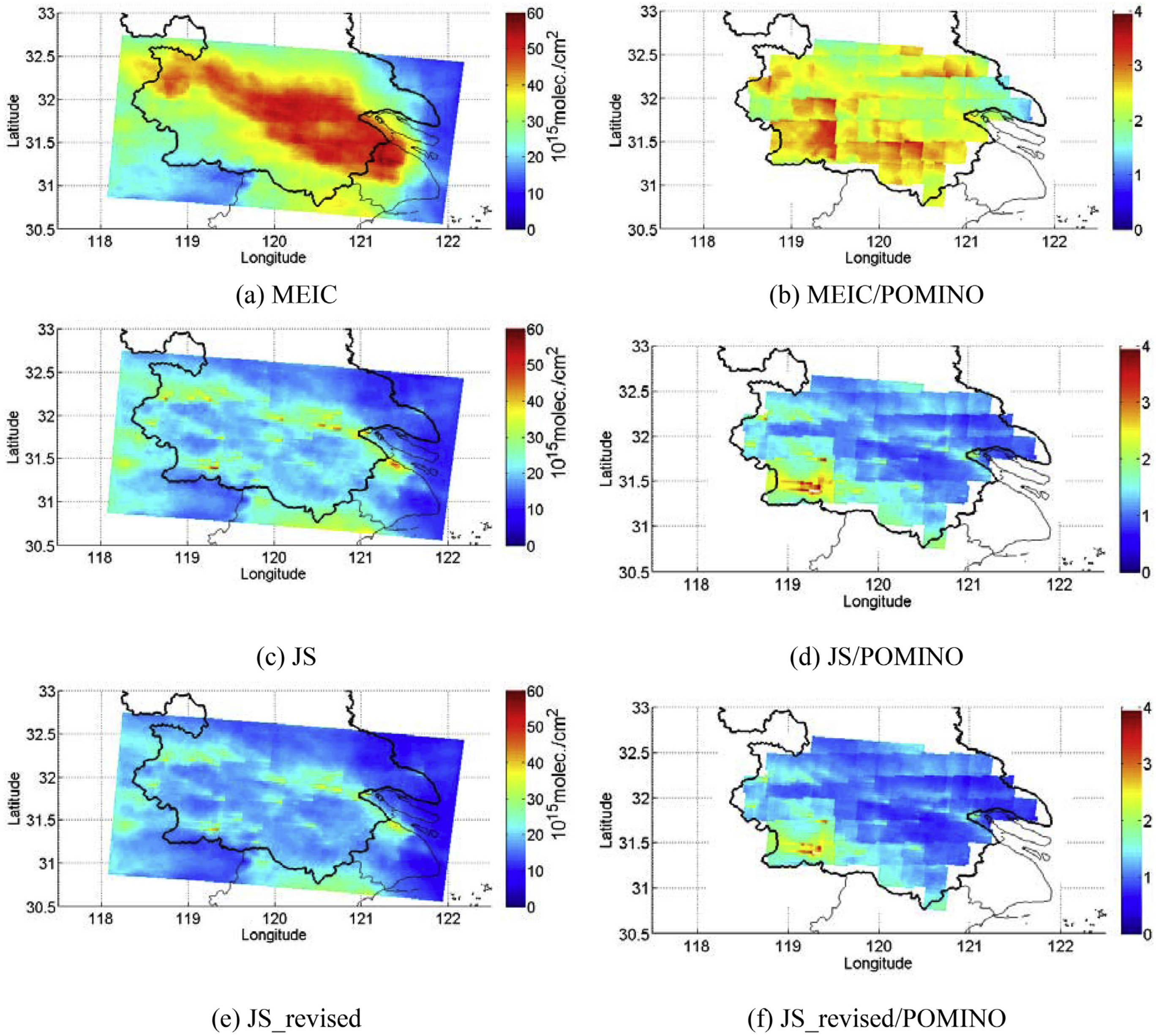

Fig. 6. The same as Fig. 5, but for April 2012.

Table 1
Model performance statistics for NO_2 VCDs from POMINO and CMAQ simulation using MEIC, JS, and JS_revised inventories in D3 (southern Jiangsu) for October 2012.

	MEIC	JS	JS_revised
R	0.42	0.44	0.58
k	2.12	1.41	1.10
RMSE (10^{15} molec./cm^2)	26.8	16.9	12.0
NME (%)	10.0	4.2	3.7

Note: The k and R are respectively the slope and correlation coefficient between the simulated and observed NO_2 VCDs through linear regression. RMSE and NME were calculated using Eqs (6) and (7), respectively.

CMAQ simulation and POMINO for October 2012, respectively, based on the data at horizontal resolution of 0.25° × 0.25°. As summarized in Table 1, there was no big difference in correlation coefficients (R) for simulated VCDs with MEIC and JS inventories, compared to satellite observations. The slopes of simulated and satellite-derived VCDs through linear regression (the k values in Table 1) were larger than 1, implying again the emissions might be overestimated in both JS and MEIC inventories, particularly for the latter one. In addition, two statistical indicators, root mean squared error (RMSE) and normalized mean error (NME), were calculated respectively with Eqs (6) and (7), and applied to evaluate the model performance:

$$RMSE = \sqrt{\frac{1}{n}\sum_{i=1}^{n}(P_i - O_i)^2} \tag{6}$$

$$NME = \frac{\sum_{i=1}^{n}|P_i - O_i|}{\sum_{i=1}^{n}O_i} \times 100\% \tag{7}$$

where P and O indicate the results from modeling prediction and observation, respectively; n is the number of data points. The smaller discrepancies between observed and simulated VCDs using JS inventory partly demonstrated the advantage of the high-resolution inventory that collected detailed information of individual sources on NO_2 simulation at provincial scale. Besides this evaluation with satellite observations, our previous study revealed that smaller discrepancies

Table 2
Wind speed (m/s) and calculated lifetime of NO_2 (h) by wind direction sector for the four cities/city combinations in southern Jiangsu. Numbers in the parentheses indicate 95% confidence intervals of lifetime.

		Nanjing	Changzhou + Wuxi	Suzhou	Zhenjiang + Yangzhou
South	Wind speed	5.08	4.95	5.47	5.03
	Lifetime	1.56 (1.29–2.02)	1.65 (1.48–2.21)	1.59 (1.94–2.36)	2.13 (1.87–2.50)
Southwest	Wind speed	5.24	5.38	5.37	5.27
	Lifetime	1.97 (1.74–2.33)	1.99 (1.82–2.21)	2.12 (1.94–2.36)	2.55 (2.18–3.18)
Northeast	Wind speed	4.8	5.47	6.07	5.73
	Lifetime	2.16 (1.94–2.47)	1.96 (1.77–2.22)	1.88 (1.79–1.98)	2.84 (2.49–3.40)

between simulated and observed surface NO_2 concentrations could also be achieved when MEIC was replaced with JS inventory in CMAQ modeling (Zhou et al., 2017). Therefore, the improvement of emission inventory for southern Jiangsu proved convincing together with CTM, ground and satellite observations.

As indicated above, the NO_X emissions in Jiangsu might be overestimated in current inventories, particularly for power sector. In 2012, SCR technologies were installed in some power plants in the province, but the actual operation conditions and benefits of NO_X control were rarely analyzed through real-time measurement due to irregular and thereby unreliable data (Liu et al., 2016b). Although the information of emission sources was collected at plant level in JS inventory, the NO_X removal rates for individual plants were commonly determined by expert judgment (e.g., data from limited investigations reported by the factory officials to local environmental protection bureaus), and the average NO_X removal efficiency for power sector was calculated at 37% for Jiangsu 2012 (Zhou et al., 2017). Based on available continuous online measurement data, however, the NO_X removal rate for certain power plants could reach 85% in the province (internal report by Jiangsu Environmental Monitoring Center), much higher than that used in JS inventory. In this work, therefore, an additional emission case, JS_revised, was developed, in which the NO_X removal rates for power plants with SCR installed were uniformly set at 85%. Such revision led to 35% reduction in NO_X emissions from power sector, and 13% reduction in the total emissions in Jiangsu. The spatial distribution of simulated NO_2 VCDs based on JS_revised and the ratio to POMINO data were illustrated in Fig. 5e and f, respectively. Reduced NO_2 VCDs were obtained compared to those using JS inventory, particularly for regions with power plants. Indicated by the slope closer to 1.0 and smaller NME (Table 1), JS_revised inventory was proved to be better in NO_2 VCD simulation. The result implies that more careful analysis on continuous emission monitoring system (CEMS) data could be a further step for emission optimization and air quality modeling at regional spatial scale.

Limitation should be acknowledged in the analysis. Sensitivity of satellite measurement decreases towards the surface, leading to uncertainty in retrieval of NO_2 VCDs and thereby in comparisons with CTM results (Eskes and Boersma, 2003; Lin et al., 2014; Lorente et al., 2017). As we applied the level-3 product of POMINO for comparison, however, averaging kernels of the product could not be directly obtained and applied in Eq. (1). Through comparison between OMI and simulated NO_2 with a global chemistry transport model, GEOS-Chem, Boersma et al. (2016) found the error of vertical sampling in satellite retrieval reached 20% and application of the averaging kernel resulted in smaller uncertainty intervals for the ratios of observed to simulated NO_2. For China, the differences were estimated moderate: the ratios of OMI to GEOS-Chem NO_2 (geometric mean) were 0.99 and 1.0 without and with averaging kernel for winter, and 1.07 and 1.13 for summer, respectively (Boersma et al., 2016). In this work, the discrepancies between simulated NO_2 using JS and MEIC inventories were larger, indicated by the slopes in Table 1. The comparison, therefore, suggested the improvement of JS inventory in simulation of NO_2 VCDs, even the uncertainty existed without application of averaging kernel. When available, application of averaging kernel for each simulated pixel is recommended for further improvement of the analysis.

3.3. Life time and top-down emissions of NO_X

Table 2 summarizes the wind speed and lifetime of NO_2 by wind direction sector for the four cities/city combinations. The average lifetimes were estimated at 1.90, 1.87, 1.86, and 2.50 h for Nanjing, Changzhou + Wuxi, Suzhou, and Zhenjiang + Yangzhou, respectively, and they were within the ranges between 1.8 and 7.5 h for NO_2 from China's power plants and cities estimated by Liu et al. (2016b). Among all the wind sectors, NO_2 lifetime under southerly was the shortest, varying from 1.18 to 2.13 for different cities. Shown in Fig. 7 are NO_2 line densities in the four cities/city combinations for the dominating wind sectors, i.e., southeast–northwest and south–north directions, based on the POMINO data in summer (May–Sep) of 2010–2014. Combining the lifetime and the constrained total mass of NO_2 with Eq. (5), the emission rates were calculated at 117.1, 221.3, 180.3, and 113.0 mol/s for Nanjing, Changzhou + Wuxi, Suzhou, and Zhenjiang + Yangzhou, respectively.

The "top-down" estimates were compared with other available bottom-up emission data, including MEIC, JS, JS_revised, and those reported in Environmental Statistics Yearbook (mentioned as ESY hereinafter; NBS and MEP, 2013), as summarized in Table 3. In particular, ESY collected detailed operation data of industrial plants and on-road vehicles, and applied them to calculate annual emissions of air pollutants including NO_X. City-level emissions were then aggregated and reported as official numbers. The statistic indicators including correlation coefficient (R), NME, and RMSE between city-level top-down and bottom-up estimates were calculated as provided in Table 3. As can be seen, most bottom-up emissions were within the ranges of ± 50% around the top-down estimates, thus the comparison mutually demonstrated the reliability of the two methods in NO_X emission calculation in southern Jiangsu. NMEs were ranged 18%–49% for different bottom-up inventories, and the results were close to that of our recent study on the uncertainty of city-level emission inventory in China (Zhao et al., 2017b). In that work, the 95% confidence interval for emissions of industrial sector in Nanjing was quantified at −10%–33% using a modified Monte-Carlo simulation framework. Among all the bottom-up estimates, JS inventory was the most consistent with the top-down estimates, indicated by the highest R and smallest NME and RMSE in Table 3. The comparison thus suggested the importance of detailed information of local sources on city-level emission estimation. The city emissions extracted from MEIC were generally larger than the top-down estimates from POMINO. Neglecting the improved use of NO_X control technologies for certain sources like power plants might be the primary reason, as mentioned earlier in Sections 3.1 and 3.2. In contrast, the ESY emissions were commonly smaller than the top-down estimates. ESY included only emissions from power, industry, and on-road transportation sector, but ignored those from off-road and residential combustion sources. Hence underestimation in total city emissions could be expected by ESY.

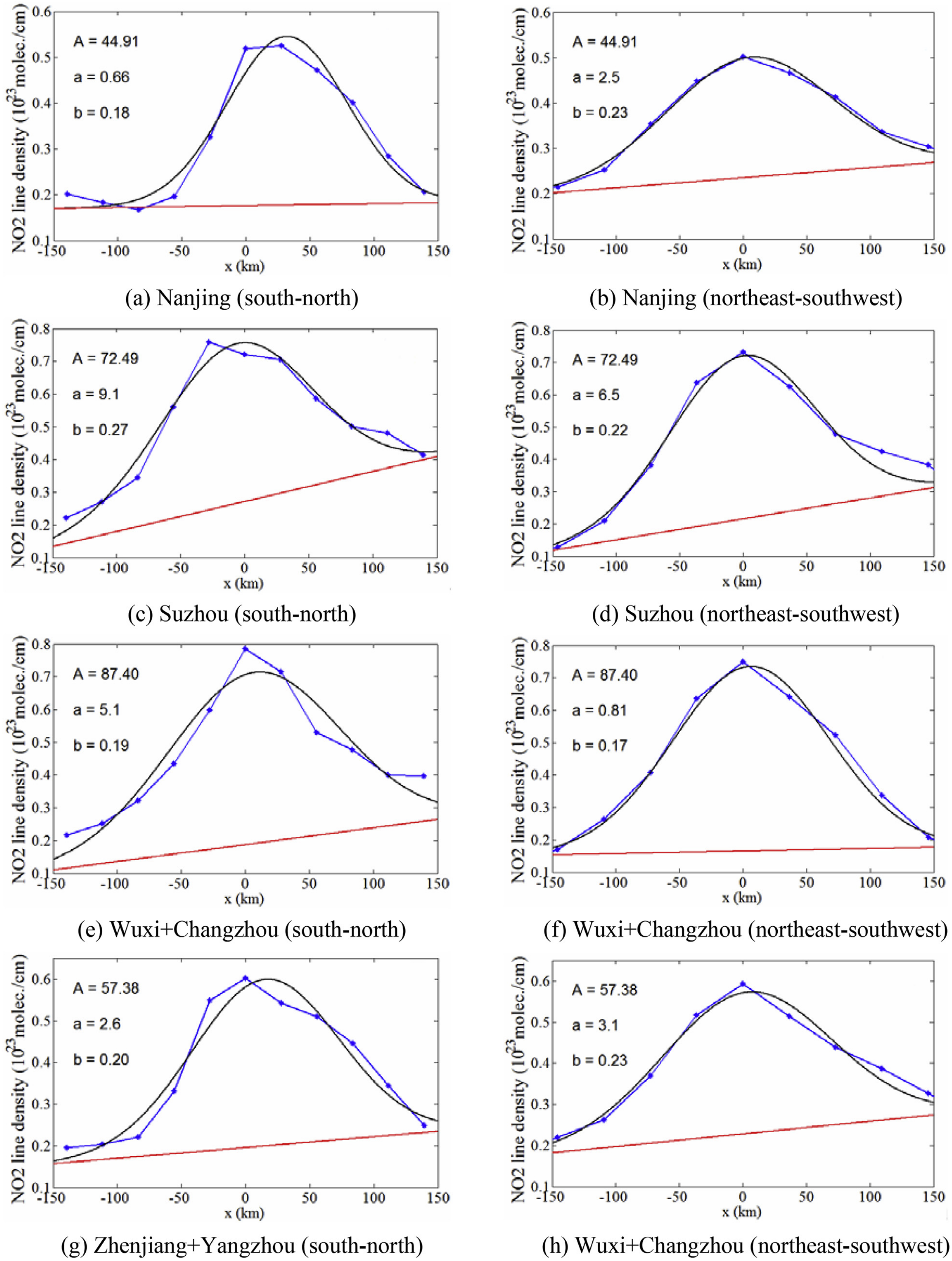

Fig. 7. NO_2 line densities in four cites/city combinations for south-north and northeast-southwest wind directions. Blue cross: NO_2 line densities for calm winds as a function of the distance to city center x; Grey line: the fit $g(x)$ (see Eq. (5)); Pink line: the fitted background $a_i + b_i x$ (see Eq. (5)). A, a and b in Eq. (5) in Eq. (5) are provided as well in each panel. (For interpretation of the references to colour in this figure legend, the reader is referred to the Web version of this article.)

Table 3
The NO_X emission rates in various bottom-up inventories and the top-down estimates with Gaussian dispersion function model for cities in southern Jiangsu. The statistics are provided as well for comparisons between bottom-up and top-down estimate.

	MEIC	JS	JS_revised	ESY	Top-down estimates
Emissions (mol/s)					
Nanjing	167.2	113.6	98.8	83.7	117.1
Wuxi + Changzhou	285.6	154.2	130.7	143	221.3
Suzhou	295.4	154	129.9	149.6	180.3
Zhenjiang + Yangzhou	192.6	98.2	84.6	96.8	113.0
Statistics					
NME (%)	49	18	30	25	–
RSME (mol/s)	81.0	36.8	54.5	46.0	–
R	0.908	0.932	0.928	0.900	–

Although it was demonstrated to be more applicable in NO_2 simulation through CTM, city emissions of JS_revised inventory was less consistent with top-down estimates, compared to those of JS inventory. Uncertainties of both bottom-up and top-down analysis should be noted. For the bottom-up JS_revised inventory, a uniform removal rate of 85% was assumed for all power plants installed with SCR technologies. Such simplified assumption might exaggerate the benefits of NO_X control for power sector, as the removal efficiencies of certain plants could not reach the assumed value. Regarding the top-down estimation, the concerned cities/city combinations were located in polluted eastern China instead of in relatively clean background regions, and the effects of interfering emission sources within small distances could not fully be eliminated using the modified method. There were possible errors in wind field simulation and satellite observations, resulting in uncertainty in emission rate estimation. For example, the deviation of wind speed and direction between ECMWF fields and sonde measurements was evaluated to result in an uncertainty of 30% for non-mountainous sites (Liu et al., 2016b). Relevant parameters for NO_2 retrieval process were obtained from CTM in POMINO, and the retrieval uncertainties associated with aerosols were estimated at 15% for both single scattering albedo and vertical distribution simulation, and that associated with vertical shape of NO_2 were 10–20% (Lin et al., 2014). According to a recent study, the NME of two top-down estimates of NO_X emissions with varied data and methods in Gaussian function model was calculated at 39.7% for selected six cites (Zhang et al., 2018). Moreover, as OMI instrument detected air pollutants with a local equator crossing time at 13:45, the retrieved NO_2 VCDs were not actually representative for diurnal mean. Discrepancy would then be expected when top-down estimation based on instant satellite observations was compared with the bottom-up inventory that stands for an average emission rate of full days. Further efforts are recommended from both bottom-up and top-down methods to reduce the discrepancy between the estimations and to thereby improve the understanding of city-level emissions in China.

4. Conclusions

Satellite-derived NO_2 VCDs from OMI were applied to evaluate different NO_X emission inventories in southern Jiangsu, combined with chemistry transport model and Gaussian function model. Through comparison between gridded NO_2 VCDs and NO_X emissions, and that between observed and simulated VCDs, advantage on air quality research was revealed for high-resolution emission inventory that incorporated the best available information of local sources. The national emission inventory MEIC was expected to overestimate NO_X emissions for Jiangsu 2012, partly because improvement in NO_X control for power sector was not fully considered in MEIC without data support from CEMS. Out of available bottom-up emission inventories, the best agreement was achieved between the high-resolution inventory at local scale and the top-down estimation from Gaussian function model based on satellite observation. To further reduce the uncertainty of the analysis, more detailed information on individual plants were recommended for emission inventory development. For example, available CEMS data indicated that emission factors of power plants in China might largely decline in recent years (internal communication with an officer of Ministry of Environmental Protection, Xin Bo). Further improvement in emission inventory could thus be expected when CEMS data are properly applied. For better analysis at provincial/city scale, products of NO_2 VCDs with finer horizontal resolution were also encouraged based on satellite observations.

Acknowledgement

This work was sponsored by the National Key Research and Development Program of China (2017YFC0210106 and 2016YFC0201507), Natural Science Foundation of China (91644220 and 41575142), and Special Research Program of Environmental Protection for Common wealth (201509004). We would like to acknowledge Qiang Zhang from Tsinghua University for the national emission data (MEIC), Jintai Lin from Peking University for POMINO data, and Fei Liu for help on top-down emission analysis. Thanks should also go to two anonymous reviewers for their very valuable comments to improve this work.

Appendix A. Supplementary data

Supplementary data related to this article can be found at https://doi.org/10.1016/j.atmosenv.2018.07.029.

References

Beirle, S., Boersma, K.F., Platt, U., Lawrence, M.G., Wagner, T., 2011. Megacity emissions and lifetimes of nitrogen oxides probed from space. Science 333, 1737–1739.
Boersma, K.F., Vinken, G.C.M., Eskes, H.J., 2016. Representativeness errors in comparing chemistry transport and chemistry climate models with satellite UV–Vis tropospheric column retrievals. Geosci. Model Dev. 9, 875–898.
Boersma, K.F., Eskes, H.J., Veefkind, J.P., Brinksma, E.J., van der A, R.J., Sneep, M., van den Oord, G.H.J., Levelt, P.F., Stammes, P., Gleason, J.F., Bucsela, E.J., 2007. Near-real time retrieval of tropospheric NO_2 from OMI. Atmos. Chem. Phys. 7, 2103–2118.
de Foy, B., Lu, Z., Streets, D.G., 2016. Impacts of control strategies, the Great Recession and weekday variations on NO_2 columns above North American cities. Atmos. Environ. 138, 74–86.
de Foy, B., Lu, Z., Streets, D.G., Lamsal, L.N., Duncan, B.N., 2015. Estimates of power plant NOx emissions and lifetimes from OMI NO_2 satellite retrievals. Atmos. Environ. 116, 1–11.
de Foy, B., Wilkins, J.L., Lu, Z., Streets, D.G., Duncan, B.N., 2014. Model evaluation of methods for estimating surface emissions and chemical lifetimes from satellite data. Atmos. Environ. 98, 66–77.
Duncan, B.N., Yoshida, Y., de Foy, B., Lamsal, L.N., Streets, D.G., Lu, Z., Pickering, K.E., Krotkov, N.A., 2013. The observed response of Ozone Monitoring Instrument (OMI) NO_2 columns to NO_X emission controls on power plants in the United States: 2005-2011. Atmos. Environ. 81, 102–111.
Eskes, H.J., Boersma, K.F., 2003. Averaging kernels for DOAS total-column satellite retrievals. Atmos. Chem. Phys. 3, 1285–1291.
Fioletov, V.E., McLinden, C.A., Krotkov, N., Li, C., 2015. Lifetimes and emissions of SO_2 from point sources estimated from OMI. Geophys. Res. Lett. 42, 1969–1976.
Fu, X., Wang, S.X., Zhao, B., Xing, J., Cheng, Z., Liu, H., Hao, J.M., 2013. Emission inventory of primary pollutants and chemical speciation in 2010 for the Yangtze River Delta region, China. Atmos. Environ. 70, 39–50.
Han, K.M., Lee, S., Chang, L.S., Song, C.H., 2015. A comparison study between CMAQ-simulated and OMI-retrieved NO_2 columns over East Asia for evaluation of NOx emission fluxes of INTEX-B, CAPSS, and REAS inventories. Atmos. Chem. Phys. 15, 1913–1938.
Krotkov, N.A., McLinden, C.A., Li, C., Lamsal, L.N., Celarier, E.A., Marchenko, S.V., Swartz, W.H., Bucsela, E.J., Joiner, J., Duncan, B.N., Boersma, K.F., Veefkind, J.P., Levelt, P.F., Fioletov, V.E., Dickerson, R.R., He, H., Lu, Z., Streets, D.G., 2016. Aura OMI observations of regional SO2 and NO2 pollution changes from 2005 to 2015. Atmos. Chem. Phys. 16, 4605–4629.
Lin, J., Martin, R.V., Boersma, K.F., Sneep, M., Stammers, P., Spurr, R., Wang, P., van Roozendael, M., Clemer, K., Irie, H., 2014. Retrieving tropospheric nitrogen dioxide from the Ozone Monitoring Instrument: effects of aerosols, surface reflectance anisotropy, and vertical profile of nitrogen dioxide. Atmos. Chem. Phys. 14, 1441–1461.

Liu, F., van der A, R.J., Eskes, H., Ding, J., Mijling, B., 2018. Evaluation of modeling NO_2 concentrations driven by satellite-derived and bottom-up emission inventories using in-situ measurements over China. Atmos. Chem. Phys. 18, 4171–4186.
Liu, F., Beirle, S., Zhang, Q., van der A, R.J., Zheng, B., Tong, D., He, K., 2017. NOx emission trends over Chinese cities estimated from OMI observations during 2005 to 2015. Atmos. Chem. Phys. 17, 9261–9275.
Liu, F., Zhang, Q., van Der A, R.J., Zheng, B., Tong, D., Yan, L., Zheng, Y., He, K., 2016a. Recent reduction in NO_X emissions over China: synthesis of satellite observations and emission inventories. Environ. Res. Lett. 11, 114002. https://doi.org/10.1088/1748-9326/11/11/114002.
Liu, F., Beirle, S., Zhang, Q., Dorner, S., He, K., Wagner, T., 2016b. NOx lifetimes and emissions of cities and power plants in polluted background estimated by satellite observations. Atmos. Chem. Phys. 16, 5283–5298.
Liu, F., Zhang, Q., Tong, D., Zheng, B., Li, M., Huo, H., He, K.B., 2015. High-resolution inventory of technologies, activities, and emissions of coal-fired power plants in China from 1990 to 2010. Atmos. Chem. Phys. 15, 13299–13317.
Lorente, A., Boersma, K.F., Yu, H., Dorner, S., Hilboll, A., Richter, A., et al., 2017. Structural uncertainty in air mass factor calculation for NO_2 and HCHO satellite retrievals. Atmos. Meas. Tech. 10, 759–782.
Lu, Z., Streets, D.G., de Foy, B., Lamsal, L.N., Duncan, B.N., Xing, J., 2015. Emissions of nitrogen oxides from US urban areas: estimation from Ozone Monitoring Instrument retrievals for 2005-2014. Atmos. Chem. Phys. 15, 10367–10383.
Lu, Z., Streets, D.G., de Foy, B., Krotkov, N.A., 2013. Ozone monitoring instrument observations of interannual increases in SO_2 emissions from Indian coal-fired power plants during 2005-2012. Environ. Sci. Technol. 13993–14000.
Mijling, B., Vander, A.R.J., Zhang, Q., 2013. Regional nitrogen oxides emission trends in East Asia observed from space. Atmos. Chem. Phys. 13, 12003–12012.
National Bureau of Statistics (NBS), 2016a. China Statistical Yearbook 2015. China Statistics Press, Beijing (in Chinese).
National Bureau of Statistics (NBS), 2016b. China Industry Economy Statistical Yearbook 2015. China Statistics Press, Beijing (in Chinese).
National Bureau of Statistics (NBS), Ministry of Environmental Protection (MEP), 2013. China Statistical Yearbook on Environment 2012. China Statistics Press, Beijing (in Chinese).
Richter, A., Burrows, J.P., Nusz, H., Granier, C., Niemeier, U., 2005. Increase in tropospheric nitrogen dioxide over China observed from space. Nature 437, 129–132.
Seinfeld, J.H., Pandis, S.N., 2006. Atmospheric Chemistry and Physics: from Air Pollution to Climate Change. John Wiley and Sons, New York, pp. 204–275.
van der A, R.J., Mijling, B., Ding, J., Koukouli, M.E., Liu, F., Li, Q., Mao, H., Theys, N., 2017. Cleaning up the air: effectiveness of air quality policy for SO_2 and NO_X emissions in China. Atmos. Chem. Phys. 17, 1775–1789.
Wang, S., Zhao, M., Xing, J., Wu, Y., Zhou, Y., Lei, Y., He, K., Fu, L., Hao, J., 2010. Quantifying the air pollutants emission reduction during the 2008 Olympic Games in Beijing. Environ. Sci. Technol. 44, 2490–2496.
Xia, Y., Zhao, Y., Nielsen, C., 2016. Benefits of China's efforts in gaseous pollutant control indicated by the bottom-up emissions and satellite observations 2000–2014. Atmos. Environ. 136, 43–53.
Zhang, J., van der A, R.J., Ding, J., 2018. Detection and emission estimates of NOx sources over China North Plain using OMI observations. Int. J. Rem. Sens. 39, 2847–2859.
Zhao, Y., Mao, P., Zhou, Y., Yang, Y., Zhang, J., Wang, S., Dong, Y., Xie, F., Yu, Y., Li, W., 2017a. Improved provincial emission inventory and speciation profiles of anthropogenic non-methane volatile organic compounds: a case study for Jiangsu, China. Atmos. Chem. Phys. 17, 7733–7756.
Zhao, Y., Zhou, Y., Qiu, L., Zhang, J., 2017b. Quantifying the uncertainties of China's emission inventory for industrial sources: from national to provincial and city scales. Atmos. Environ. 165, 207–221.
Zhao, Y., Zhang, J., Nielsen, C., 2014. The effects of energy paths and emission controls and standards on future trends in China's emissions of primary air pollutants. Atmos. Chem. Phys. 14, 8849–8868.
Zhao, Y., Qiu, L., Xu, R., Xie, F., Zhang, Q., Yu, Y., Nielsen, C.P., Qin, H., Wang, H., Wu, X., Li, W., Zhang, J., 2015. Advantages of a city-scale emission inventory for urban air quality research and policy: the case of Nanjing, a typical industrial city in the Yangtze River Delta, China. Atmos. Chem. Phys. 15, 12623–12644.
Zheng, J., Zhang, L., Che, W., Zheng, Z., Yin, S., 2009. A highly resolved temporal and spatial air pollutant emission inventory for the Pearl River Delta region, China and its uncertainty assessment. Atmos. Environ. 43, 5112–5122.
Zhou, Y., Zhao, Y., Mao, P., Zhang, Q., Zhang, J., Qiu, L., Yang, Y., 2017. Development of a high-resolution emission inventory and its evaluation and application through air quality modeling for Jiangsu Province, China. Atmos. Chem. Phys. 17, 211–233.